NANO LETTERS

Letter

pubs.acs.org/NanoLett

Metastable Growth of Pure Wurtzite InGaAs Microstructures

Kar Wei Ng, Wai Son Ko, Fanglu Lu, and Connie J. Chang-Hasnain*

Department of Electrical Engineering and Computer Sciences, University of California at Berkeley, Berkeley, California 94720, United States

ABSTRACT: III−V compound semiconductors can exist in two major crystal phases, namely, zincblende (ZB) and wurtzite (WZ). While ZB is thermodynamically favorable in conventional III−V epitaxy, the pure WZ phase can be stable in nanowires with diameters smaller than certain critical values. However, thin nanowires are more vulnerable to surface recombination, and this can ultimately limit their performances as practical devices. In this work, we study a metastable growth mechanism that can yield purely WZ-phased InGaAs microstructures on silicon. InGaAs nucleates as sharp nanoneedles and expand along both axial and radial directions simultaneously in a core−shell fashion. While the base can scale from tens of nanometers to over a micron, the tip can remain sharp over the entire growth. The sharpness maintains a high local surface-to-volume ratio, favoring hexagonal lattice to grow axially. These unique features lead to the formation of microsized pure WZ InGaAs structures on silicon. To verify that the WZ microstructures are truly metastable, we demonstrate, for the first time, the in situ transformation from WZ to the energy-favorable ZB phase inside a transmission electron microscope. This unconventional core−shell growth mechanism can potentially be applied to other III−V materials systems, enabling the effective utilization of the extraordinary properties of the metastable wurtzite crystals.

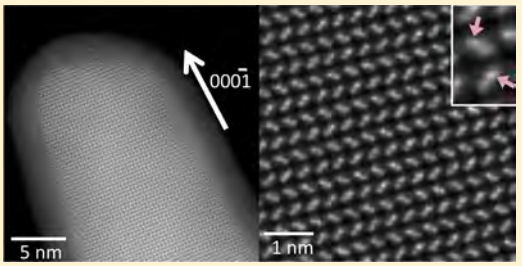

KEYWORDS: *Nanowire, III−V, core−shell, wurtzite, phase purity*

III−V semiconductors have been the fundamental building blocks for high-performance optoelectronic devices and transistors due to their superior optical and electrical properties. There are two main crystal phases in the binary octet semiconductors, namely, zincblende (ZB) and wurtzite (WZ). Except for the nitride system, bulk III−V epitaxial films usually exist in the ZB crystal phase. This can be attributed to the relatively low ionicity in most III−V compounds. The highly covalent nature favors a staggered configuration in which electrostatic repulsion from the third nearest neighbor is minimized.[1] Rigorous calculations using local-density formalism show that WZ structures have higher free energy than their ZB counterparts in most III−V materials.[2] As a result, the cubic ZB structure has been the energy-preferable crystal phase in arsenide and phosphide material systems.

Crystal stability can be significantly different at nanometer scales. As the crystal size shrinks, surface energy becomes an important factor in determining the total free energy change for crystal formation. Studies have shown that WZ crystals exhibit lower surface energies than ZB lattices.[3] This implies that WZ can become thermodynamically favorable when the surface-to-volume ratio of the nanostructures becomes sufficiently large. Indeed, single crystal wurtzite nanowires have been experimentally demonstrated in various material systems via catalytic vapor−liquid−solid (VLS) growth or selective area epitaxy.[4−9] These nanostructures exhibit unusual optoelectronic properties due to their unique crystal symmetry dissimilar to their bulk lattice.[10−12] For instance, GaP, an indirect bandgap material in cubic phase, becomes direct bandgap in WZ-phased nanowires synthesized by VLS.[5] With further tailoring in the alloy composition, these WZ nanowires can potentially be used as efficient green emitters on silicon. To make efficient devices, however, it is crucial to minimize surface-assisted nonradiative recombinations by proper surface passivation and increasing the nanowire size. Unfortunately, there exists a critical diameter (usually <50 nm) above which WZ phase becomes unstable such that the nanostructure evolves into a mixture of cubic and hexagonal lattices.[3,13,14] This inevitably limits the size and ultimately the optical performance of the extraordinary crystals.

Recently, we demonstrated the unconventional growth of GaAs, InGaAs, and InP nanoneedles and pillars on silicon, poly silicon, and sapphire substrates.[15−18] Despite a lattice mismatch as large as 46%, the III−V structures can be scaled into micron size without compromising the crystal quality. Most shockingly, these microstructures are in pure WZ crystal lattice even when the base diameter is above 1 μm, which is more than 20 times over the nanowire critical limit. In this paper, we aim to explain how this metastable growth occurs. While the nucleation is likely assisted by group-III nanoclusters, InGaAs/GaAs needles expand in a core−shell fashion without any metal catalyst observed at the extremely sharp tip. Notably, the nanostructures expand in both radial and axial directions simultaneously, dissimilar to most nanowire work. These two independent growth components enable the base to expand freely from tens of nanometers to over a micron while the tip can remain sharp (<20 nm in diameter) at the same time. This extraordinary

Received: May 21, 2014
Revised: June 29, 2014
Published: July 2, 2014

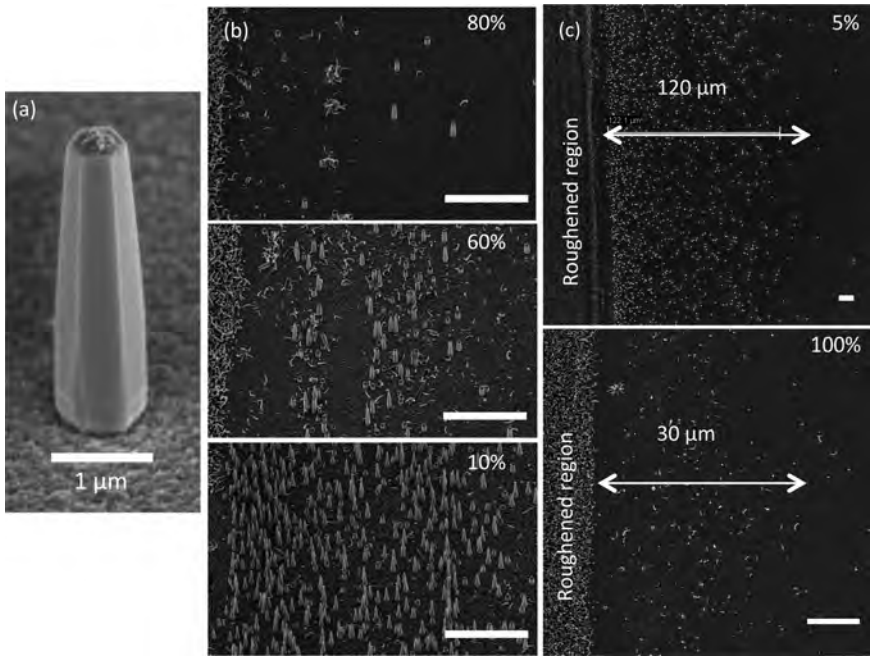

Figure 1. (a) SEM image of a typical InGaAs/GaAs core−shell pillar with a base diameter approaching a micron. (b) Pillar density increases as the V/III ratio decreases from 80% to 10%, where 100% represents a V/III ratio of 43. (c) Micropillars nucleate at locations much further away from the roughened region when the V/III ratio reduces from 100% to 5%. Scale bars in b and c represent 10 μm.

combination turns out to be the key for the metastable growth of microneedles and pillars. Finally, we demonstrate the in situ phase transformation from WZ to ZB inside a transmission electron microscope (TEM). With further improvements in experimental design, direct measurement of the energy difference between the two crystal phases may be possible.

$In_{0.2}Ga_{0.8}As$/GaAs core−shell micropillars are synthesized directly on (111)-Si substrates via metal−organic chemical vapor deposition (MOCVD) at 400 °C. Details of the growth can be found in our previous work.[19] Notably, the substrates were roughened mechanically to facilitate seeding of micropillars. Figure 1a is a scanning electron microscope (SEM) image displaying a typical pillar with base diameter approaching 1 μm. The well-faceted hexagonal shape and smooth sidewall are the first indication of excellent crystal quality. As reported previously, the III−V structures nucleate as sharp nanoneedles.[20] The growth then proceeds in a core−shell fashion in which the nanoneedles expand along the axial and radial directions simultaneously. While lateral growth occurs continuously throughout the entire process, growth along the vertical direction saturates at a long growth time. This turns the originally sharp nanoneedle into blunt micropillars. The independence of axial and radial growths is the key for the metastable growth and will be discussed in more detail shortly.

To study how the metastable growth starts, a series of samples were grown under various V/III ratios. Figure 1b illustrates the dependence of pillar density on the V/III ratio. Tertiary butylarsine (TBAs) was used as the precursor of arsenic. Under the same group III flow rates, micropillar density increases drastically with reduced TBAs flow. In addition, the pillars nucleate at locations much further away from the roughened region under lower TBAs flow. Figure 1c reveals that pillar nucleation extends to over 120 μm away from the roughened region when the TBAs flow is cut down by 20 times. These observations suggest that micropillar nucleation is significantly promoted by longer group III diffusion lengths, which are highly sensitive to the V/III ratio.[21] We hypothesize that the seeding of micropillars begins with the formation of metal nanoclusters at the roughened region. Mechanical roughening not only creates an uneven surface morphology but also opens up fresh silicon surface for oxidation. Since III−V cannot nucleate on top of native oxide, group III adatoms tend to cluster into very small droplets on the porous oxide at the very early stage. These nanodroplets diffuse away from the roughened regions to flat silicon surface and react with As adatoms to form InGaAs nanocrystals. The high supersaturation of adatoms favor the formation of WZ nanostructures with high aspect ratios, which later on evolve into InGaAs needles and pillars.[22] A reduction in TBAs flow increases the diffusion length of group III adatoms, thus enhancing the formation and diffusion of metal nanoclusters during the nucleation phase. This metal-initiated nucleation hypothesis fits well with the observed dependence of density and nucleation distance on the V/III ratio in Figure 1.

Although metal nanoclusters are likely involved in nucleation, the growth mechanism presented in this work is different from VLS growth. In the latter case, a metal catalyst is needed to dissolve the reactants and stays at the tip of the nanowire throughout the entire growth.[23,24] In our growth, however, no metal catalyst is ever observed at the tip of the nanostructure. We believe that the metal seed is completely consumed for the initial nanoneedle formation and the subsequent growth is in a pure core−shell fashion. Another major difference is that the nanowire diameter grown by VLS is predefined by the catalyst size. If the catalyst size exceeds the critical diameter, the whole nanowire becomes polytypic. In the nanoneedle growth, however, the base diameter scales linearly with time.[20] This freedom in lateral expansion is in fact the key factor for the metastable WZ growth. The metal initiated core−shell growth presented in this work is truly a unique mechanism that enables high-quality and sizable growth of microstructures on mismatched substrates.

dx.doi.org/10.1021/nl501887f | Nano Lett. 2014, 14, 4757−4762

Crystal polarity plays an important role in the stability of nanostructures. Studies have shown that nanowires are usually stabilized with a group V terminated (or (111)B-terminated) top facet.[25] To study the polarity of the microstructures in this work, we examine the tip of sharp as-grown InGaAs/GaAs core−shell needles using a transmission electron aberration corrected microscope (TEAM). Sample preparation involves simple transfer of nanoneedles mechanically from the silicon substrates to a TEM copper grid. Figure 2a shows a high-angle annular dark field (HAADF) image of a typical InGaAs/GaAs core−shell needle. Wurtzite lattice is found to extend all the way up to the tip, which is wrapped around by a thin native oxide. No sign of any metal droplet can be seen on the top surface, in sharp contrast to VLS nanowires. Notably, the tip is composed of pure GaAs since the InGaAs core is completely embedded within the shell in all directions (see schematic in Figure 3a). Figure 2b displays a magnified image of the binary compound showing characteristic zigzag crystal lattice. Since As has a slightly higher atomic number than Ga, the former appears to be brighter in a *z*-contrast HAADF image. Despite the subtle contrast difference, we can see that the top atomic column shows higher intensity than the bottom one in each "dumbbell" (see inset of Figure 2b). This indicates that the nanostructure is terminated with As plane, or $(000\bar{1})$ plane, at the top facet. This group V termination behavior is consistent with other nanowire work.

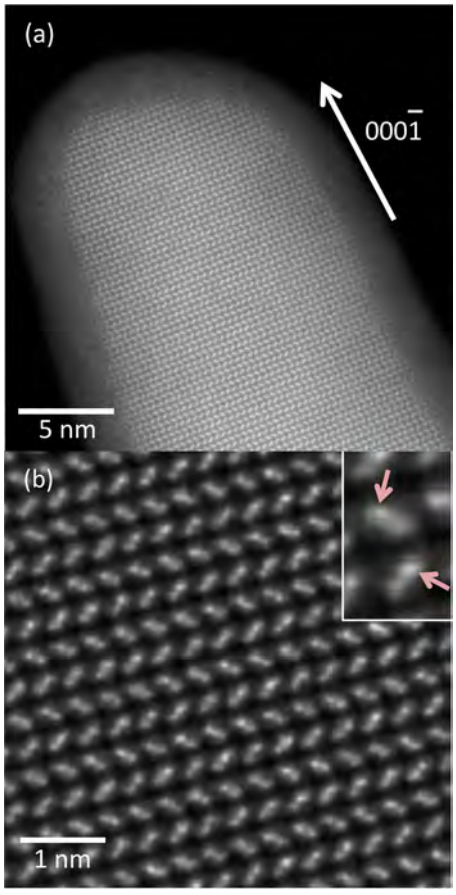

Figure 2. (a) HAADF image showing the tip of an InGaAs/GaAs nanoneedle. No metal catalyst is seen on the extremely sharp tip with ~5 nm in diameter. (b) Magnified image showing the zigzag lattice arrangement. The inset shows two Ga−As "dumbbells". The top atomic column (indicated by arrows) in each Ga−As pair is brighter than the bottom one, showing that the needle top facet is As-terminated.

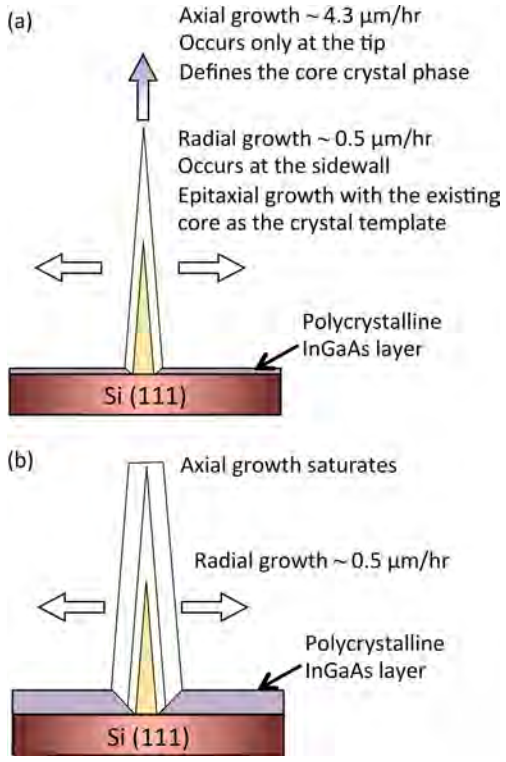

Figure 3. (a) Schematic illustration showing the different components in the core−shell growth of nanoneedles. (b) In blunt pillars, axial growth saturates, while radial growth continues with a growth rate similar as before.

The core−shell growth mechanism in this work enables expansions along both axial and radial direction simultaneously, as schematically illustrated in Figure 3a. This is dissimilar to other nanowire work, in which the growth is usually dominated along one direction. Notably, the microstructures start as sharp nanoneedles and evolve into blunt pillars at long growth times. There are two implications with this phenomenon. First, the two growth components are relatively independent since lateral growth continues even after vertical growth stops. Second, vertical growth occurs only at the very tip of the nanostructure. Otherwise, the nanostructure would not have expanded in the horizontal direction only after vertical growth stops at the tip. Figure 3 illustrates how these two growth components occur in needles and pillars. We believe that both components are crucial to the formation of microsized single-WZ-phased structures. Lateral growth is a layer-by-layer growth similar to normal thin film epitaxy. The freshly deposited layer simply follows the crystal lattice of the core. Since the core is in WZ phase, the subsequent deposition also assumes a WZ lattice arrangement. In other words, lateral growth effectively increases the volume of the wurtzite-phased crystal. As the size increases, the surface-to-volume ratio reduces, and the crystal would be more stable in the ZB phase. However, a large amount of energy is necessary to break bonds and convert the entire bulk material back into the energy-preferred ZB phase. This energy barrier keeps the nanostructure stable in WZ phase even when the size is well beyond the critical diameter.

Vertical growth, on the other hand, is a completely different story. While lateral growth is simply a copy of the core's lattice,

dx.doi.org/10.1021/nl501887f | *Nano Lett.* 2014, 14, 4757−4762

vertical growth creates the core for subsequent horizontal expansion. Growth along *c*-axis involves the deposition of basal planes whose stacking sequence defines the crystal phase of the freshly deposited material. Since ZB and WZ share the same basal plane, stacking the new layers in ABAB or ABCA can be relatively independent of the crystal underneath. While sharp nanoneedle exhibits pure WZ phase all the way up to the tip (see Figure 2), blunt pillars are terminated with cubic layers, as reported in our previous work.[20] We believe that the extraordinary sharpness of the nanoneedle tip is the driving force for the WZ phase to dominate along the vertical direction. The sharpness maintains a large local sidewall-surface-to-volume ratio at the tip. Experimentally, we always observe that the nanoneedle sidewalls are composed of $\{1\bar{1}00\}$ facets. To form ZB lattice on top of a WZ template, the overgrown crystal has to follow the crystallographic relations between the two crystal phases, i.e., ZB $\langle 110\rangle$ // WZ $<11\bar{2}0>$ and ZB $\langle 211\rangle$//WZ $<1\bar{1}00>$. Therefore, the cubic crystal has to terminate with {211} facets due to the WZ lattice template underneath, although {110} are theoretically shown to have lower surface energy than {211}.[26,27] The large local sidewall-surface-to-volume ratio at the sharp tip thus favors the formation of WZ phase since WZ $\{1\bar{1}00\}$ has lower surface energy than ZB {211}.[3] However, vertical growth slows down as the nanoneedle length increases, probably due to reduced group-III supply through the diffusion of adatoms. While lateral growth remains relatively constant throughout the growth, a slower vertical growth results in thickening of the tip. In other words, the top facet, which is composed of the c-plane, increases in diameter. A large top facet, however, does not benefit the growth of WZ crystal, as ZB {111} should have a very similar surface energy as WZ (0001). The net result is that the effective sidewall-surface-to-volume ratio at the thicker tip reduces, making WZ phase less energy favorable. Eventually, when the top facet exceeds a certain diameter, the ZB phase becomes more thermodynamically stable. This triggers the onset of vertical termination, resulting in the formation of blunt pillar structures.

In InGaAs nanoneedles, the vertical and lateral growth rates are 4.3 μm/h and 0.5 μm/h, respectively. This growth rate anisotropy brings about the extreme sharpness observed in the InGaAs nanostructure. The origin of the ultra fast vertical growth is probably the rich supply of adatoms which diffuse from the substrate and/or nanoneedle sidewall to the tip. To study how vertical growth is affected by adatom diffusion, we grew a series of InGaAs/GaAs core−shell nanostructures under various V/III ratios, as displayed in Figure 4. Notably, the flow rates of group III precursors were held constant in the experiments. While the base diameter (i.e., lateral growth) is not sensitive to group V partial pressure, the nanopillar length is observed to increase gradually with reducing TBAs flow. At an extremely low V/III ratio, the nanostructure remains as sharp needles with length exceeding 4 μm. We attribute this phenomenon to the promoted diffusion of group III adatoms under a low V/III ratio. The longer diffusion length delays the onset of vertical growth saturation, thus leading to the observed trend in Figure 4. These results show that the growth along *c*-axis is indeed highly dependent on diffusion flux of adatoms.

So far we have identified the different growth components that enable InGaAs to expand into hexagonal microstructures. Although the ZB phase is more energy favorable in the micron-size regime, the large energy barrier prevents bulk WZ lattice from converting into the thermodynamically preferred crystal

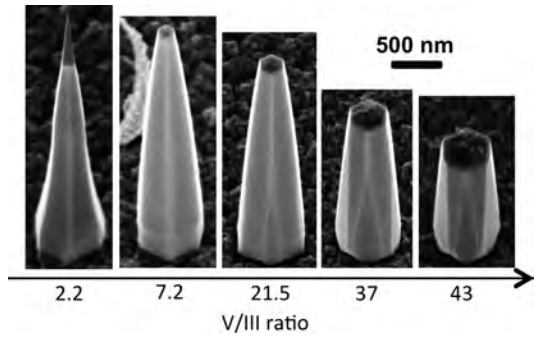

Figure 4. Dependence of pillar/needle length on V/III ratios. All nanostructures consist of a 68 min InGaAs core embedded inside a 24 min GaAs shell. SEM images were taken at 30° tilt angle. The length of the nanostructure increases with reducing the V/III ratio, and ultimately a sharp needle is obtained when the V/III ratio reaches 2.2. The tip of the sharp needle, composed of pure GaAs, appears darker than the bulk material which contains indium.

phase. Theoretically, crystal phase transformation is possible if a huge amount of energy is supplied to the nanopillar. Here, we experimentally demonstrate this transformation in situ in a FEI CM-300 TEM. Figure 5a shows a bright field TEM image of a blunt InGaAs pillar mechanically detached from the substrate. Except the very tip of the pillar, the entire structure is in the WZ phase, as attested by the clearly discernible selective area diffraction pattern (SADP) shown in Figure 5b, taken along the $[11\bar{2}0]$ zone axis. Figure 5c shows a close-up image of the pillar tip. Atop the pillar top facet, there exists an irregular feature which is a poly crystal that nucleates on the blunt pillar top at the later stage of the growth. Such polycrystalline structure can also be seen in blunt pillars with large-area top facets in Figure 4. Nevertheless, no stacking disorders or other defects can be seen in the pillar below the poly crystal. Under high resolution (Figure 5d), the WZ pillar is found to terminate with a few cubic layers as a result of vertical growth saturation. To initiate the phase transformation, we condensed the electron beam onto the nanopillar base for 5 s to deliver a high-energy dose. As seen in Figure 5e, the nanopillar tip becomes considerably deformed after the energy blast. Horizontal stacking disorders are observed to evolve at the tip after the high-energy process. SADP taken at the tip (see Figure 5f) now shows two sets of diffraction patterns along the ZB [110] zone axis instead of the WZ diffractions in Figure 5b. The two sets of diffractions originate from rotational twinning of ZB crystals with $(1\bar{1}1)$ as the mirror plane. The information extracted from the diffraction pattern agrees well with the high-resolution TEM (HRTEM) image shown in Figure 5g. A single phase ZB section is observed in the topmost ∼10 nm, followed by a bottom portion populated with twins and stacking faults. Such an observation confirms the transformation of the original hexagonal lattice into cubic lattice. Notably, only the top-most ∼140 nm turns into cubic lattice in Figure 5e. We believe that the incident electron beam on the pillar created an electric current which flowed toward the tip in a way similar to the lightning rod effect. These charge carriers accumulated at the tip and finally discharged, creating locally confined heat that is large enough to overcome the energy barrier for phase transformation. Since the heating was not well-controlled, stacking disorders and twinning were induced during the transition. In particular, the WZ-to-ZB transition seems not to be a very exothermic process, or otherwise the heat produced in

dx.doi.org/10.1021/nl501887f | *Nano Lett.* 2014, 14, 4757−4762

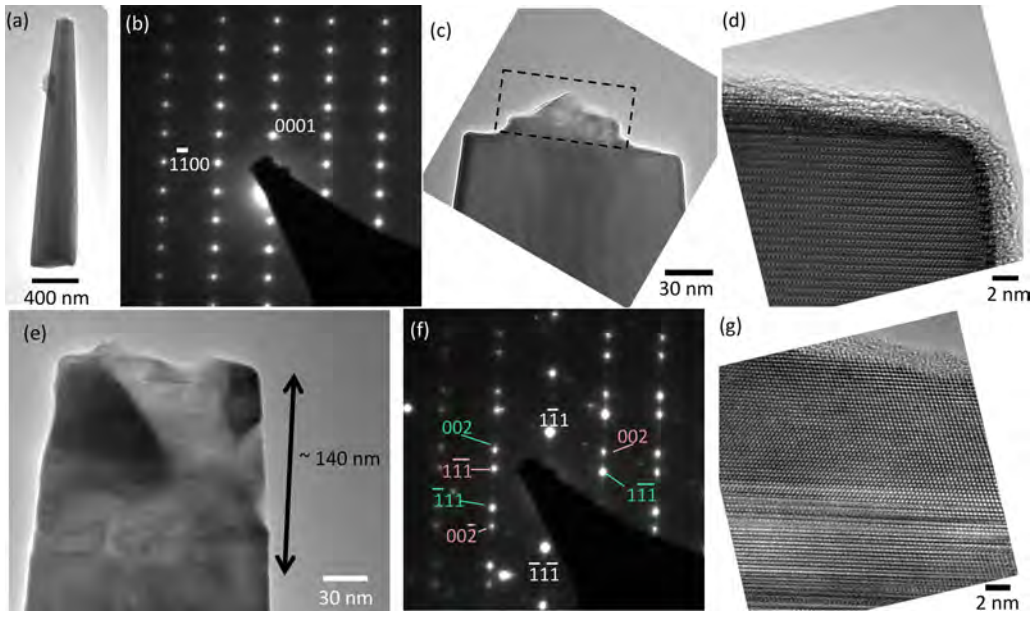

Figure 5. (a) Bright field TEM image of a blunt InGaAs pillar. (b) SADP of the pillar taken along [11−20] zone axis. (c) Close-up of the pillar tip. The structure enclosed in the dotted line box is a poly crystal nucleating on the flat top facet at the later stage of the growth. (d) HRTEM image at the tip. The WZ lattice is terminated with a few cubic layers. (e) The pillar tip after large energy dose. The topmost ~140 nm is transformed into cubic lattice with frequent stacking disorders and twinning. (f) SADP taken at the pillar tip after the energy dose. Two sets of diffraction patterns (labeled in red and green) along [110] zone axis are seen as a result of ZB twins. (g) HRTEM at the very tip. Single phase ZB lattice is observed in the top-most 10 nm.

the reaction should trigger further phase change below the topmost ~140 nm. This suggests that the net heat produced in the reaction, or in other words the energy difference between bulk WZ and ZB, may not be very large. Notably, the experiment was carried out in a single beam TEM such that the transformation process could not be monitored in real time when the beam was condensed to deliver the power impulse. With a dual-beam system like the TEAM 0.5, it is possible to quantitatively evaluate the energy required for the WZ-to-ZB transformation. Nevertheless, this in situ experiment is a first demonstration showing that the WZ phase InGaAs nanopillars can be fairly stable and a large amount of energy is needed to transform the metastable lattice into the most energy-preferred cubic phase.

In summary, we explored how InGaAs microstructures can stabilize in pure WZ phase when the base diameter is 20 times over the critical value for nanowires. The growth starts with metal-assisted nucleation, followed by layer-by-layer core−shell growth. HRTEM shows that metal droplet is completely absent at the needle tip, attesting to the catalyst-free nature of the growth. The sharp tip maintains a high local surface-to-volume ratio which favors WZ crystal formation along the axial direction. Lateral growth, on the other hand, allows the base to scale linearly with time, thus leading to the growth of WZ phase microstructure. In situ phase transition from WZ to thermodynamically stable ZB was demonstrated for the first time. With further optimization in experiment design, direct measurement of the energy difference between the two phases may be possible. We believe that the core−shell growth mechanism is not limited to InGaAs and InP, but also applicable to other III−V materials systems. This can potentially enable the effective utilization of the unique optoelectronic properties of the metastable wurtzite crystals.

AUTHOR INFORMATION

Corresponding Author

*E-mail: cch@berkeley.edu.

Notes

The authors declare no competing financial interest.

ACKNOWLEDGMENTS

This work was supported by U.S. DOE Sunshot Program (DE-EE0005316), DoD NSSEFF Fellowship (N00244-09-1-0013 and N00244-09-1-0080), and the Center for Energy Efficient Electronics Science (NSF Award 0939514). We acknowledge support of the National Center for Electron Microscopy, LBL, which is supported by the U.S. DOE (DE-AC02-05CH1123).

REFERENCES

(1) Lawaetz, P. Stability of Wurtzite Structure. *Phys. Rev. B* **1972**, *5* (10), 4039−4045.

(2) Yeh, C. Y.; Lu, Z. W.; Froyen, S.; Zunger, A. Zinc-blende-wurtzite polytypism in semiconductors. *Phys. Rev. B* **1972**, *46* (16), 10086−10097.

(3) Dubrovskii, V. G.; Sibirev, N. V. Growth thermodynamics of nanowires and its application to polytypism of zinc blende III-V nanowires. *Phys. Rev. B* **2008**, *77*, 035414−8.

(4) Spirkoska, D.; Arbiol, J.; Gustafsson, A.; Conesa-Boj, S.; Glas, F.; Zardo, I.; Heigoldt, M.; Gass, M. H.; Bleloch, A. L.; Estrade, S.; Kaniber, M.; Rossler, J.; Peiro, F.; Morante, J. R.; Abstreiter, G.; Samuelson, L.; Fontcuberta i Morral, A. Structural and optical properties of high quality zinc-blende/wurtzite GaAs nanowire heterostructures. *Phys. Rev. B* **2009**, *80*, 245325.

(5) Assali, S.; Zardo, I.; Plissard, S.; Kriegner, D.; Verheijen, M. A.; Bauer, G.; Meijerink, A.; Belabbes, A.; Bechstedt, F.; Haverkort, J. E. M.; Bakkers, E. P. A. M. Direct Band Gap Wurtzite Gallium Phosphide Nanowires. *Nano Lett.* **2013**, *13*, 1559−1563.

(6) Ahtapodov, L.; Todorovic, J.; Olk, P.; Mjåland, T.; Slåttnes, P.; Dheeraj, D. L.; van Helvoort, A. T. J.; Fimland, B.-O.; Weman, H. A

Story Told by a Single Nanowire: Optical Properties of Wurtzite GaAs. *Nano Lett.* **2012**, *12*, 6090−6095.
(7) Crankshaw, S.; Reitzenstein, S.; Chuang, L. C.; Moewe, M.; Münch, S.; Böckler, C.; Forchel, A.; Chang-Hasnain, C. Recombination dynamics in wurtzite InP nanowires. *Phys. Rev. B* **2008**, *77*, 235409.
(8) Kitauchi, Y.; Kobayashi, Y.; Tomioka, K.; Hara, S.; Hiruma, K.; Fukui, T.; Motohisa, J. Structural Transition in Indium Phosphide Nanowires. *Nano Lett.* **2010**, *10*, 1699−1703.
(9) Funk, S.; Li, A.; Ercolani, D.; Gemmi, M.; Sorba, L.; Zardo, I. Crystal Phase Induced Bandgap Modifications in AlAs Nanowires Probed by Resonant Raman Spectroscopy. *ACS Nano* **2013**, *7*, 1400−1407.
(10) De, A.; Pryor, C. E. Optical dielectric functions of wurtzite III-V semiconductors. *Phys. Rev. B* **2012**, *85*, 125201.
(11) Chen, R.; Crankshaw, S.; Tran, T.; Chuang, L. C.; Moewe, M.; Chang-Hasnain, C. Second-harmonic generation from a single wurtzite GaAs nanoneedle. *Appl. Phys. Lett.* **2010**, *96*, 051110.
(12) Li, K.; Sun, H.; Ren, F.; Ng, K. W.; Tran, T. T. D.; Chen, R.; Chang-Hasnain, C. J. Tailoring the Optical Characteristics of Microsized InP Nanoneedles Directly Grown on Silicon. *Nano Lett.* **2014**, *14*, 183−190.
(13) Akiyama, T.; Sano, K.; Nakamura, K.; Ito, T. An Empirical Potential Approach to Wurtzite−Zinc-Blende Polytypism in Group III−V Semiconductor Nanowires. *Jpn. J. Appl. Phys.* **2006**, *45*, L275.
(14) Chuang, L. C.; Moewe, M.; Chase, C.; Kobayashi, N. P.; Chang-Hasnain, C. J.; Crankshaw, S. Critical Diameter for III-V Nanowires Grown on Lattice-Mismatched Substrates. *Appl. Phys. Lett.* **2007**, *90*, 043115.
(15) Moewe, M.; Chuang, L. C.; Crankshaw, S.; Chase, C.; Chang-Hasnain, C. J. Atomically sharp catalyst-free wurtzite GaAs/AlGaAs nanoneedles grown on silicon. *Appl. Phys. Lett.* **2008**, *93*, 23116.
(16) Ren, F.; Ng, K. W.; Li, K.; Sun, H.; Chang-Hasnain, C. J. High-quality InP nanoneedles grown on silicon. *Appl. Phys. Lett.* **2013**, *102*, 012115.
(17) Chuang, L. C.; Moewe, M.; Ng, K. W.; Tran, T. T. D.; Crankshaw, S.; Chen, R.; Ko, W. S.; Chang-Hasnain, C. J. GaAs nanoneedles grown on sapphire. *Appl. Phys. Lett.* **2011**, *98*, 123101.
(18) Ng, K. W.; Tran, T. T. D.; Ko, W. S.; Chen, R.; Lu, F.; Chang-Hasnain, C. J. Single Crystalline InGaAs Nanopillar Grown on Polysilicon with Dimensions beyond the Substrates Grain Size Limit. *Nano Lett.* **2013**, *13*, 5931−5937.
(19) Chen, R.; Tran, T. T. D.; Ng, K. W.; Ko, W. S.; Chuang, L. C.; Sedgwick, F. G.; Chang-Hasnain, C. J. Nanolasers Grown on Silicon. *Nat. Photonics* **2011**, *5*, 170−175.
(20) Ng, K. W.; Ko, W. S.; Tran, T. T. D.; Chen, R.; Nazarenko, M. V.; Lu, F.; Dubrovskii, V. G.; Kamp, M.; Forchel, A.; Chang-Hasnain, C. J. Unconventional Growth Mechanism for Monolithic Integration of III−V on Silicon. *ACS Nano* **2013**, *7*, 100−107.
(21) Nishinaga, T.; Shen, X. Q.; Kishimoto, D. Surface diffusion length of cation incorporation studied by microprobe-RHEED/SEM MBE. *J. Cryst. Growth* **1996**, *163*, 60−66.
(22) Dubrovskii, V. G.; Sibirev, N. V.; Zhang, X.; Suris, A. A. Stress-Driven Nucleation of Three-Dimensional Crystal Islands: From Quantum Dots to Nanoneedles. *Cryst. Growth Des.* **2010**, *10*, 3949−3955.
(23) Cirlin, G. E.; Dubrovskii, V. G.; Samsonenko, Y. B.; Bouravleuv, A. D.; Durose, K.; Proskuryakov, Y. Y.; Mendes, B.; Bowen, L.; Kaliteevski, M. A.; Abram, R. A.; Zeze, D. Self-catalyzed, pure zincblende GaAs nanowires grown on Si(111) by molecular beam epitaxy. *Phys. Rev. B* **2010**, *82*, 035302.
(24) Hillerich, K.; Dick, K. A.; Messing, M. E.; Deppert, K.; Johansson, J. Simultaneous growth mechanisms for Cu-seeded InP nanowires. *Nano Res.* **2012**, *5*, 297−306.
(25) Tomioka, K.; Tanaka, T.; Hara, S.; Hiruma, K.; Fukui, T. III−V Nanowires on Si Substrate: Selective-Area Growth and Device Applications. *IEEE J. Sel. Top. Quant.* **2011**, *17*, 1112−1129.
(26) Pankoke, V.; Kratzer, P.; Sakong, S. Calculation of the diameter-dependent polytypism in GaAs nanowires from an atomic motif expansion of the formation energy. *Phys. Rev. B* **2011**, *84*, 075455.
(27) Sibirev, N. V.; Timofeeva, M. A.; Bolshakov, A. D.; Nazarenko, M. V.; Dubrovskii, V. G. Surface Energy and Crystal Structure of Nanowhiskers of III-V Semiconductor Compounds. *Phys. Solid State* **2010**, *52*, 1428.